

Towards Understanding the Origin of Cosmic Ray Electrons with Precision Results from AMS on ISS

Weiwei Xu*

Shandong University

for the AMS-02 Collaboration[†]

E-mail: Weiwei.Xu@CERN.CH

The precision measurements of the cosmic ray electron flux in the energy range from 0.5 GeV to 1.4 TeV based on 28.1 million electrons collected by the Alpha Magnetic Spectrometer on the International Space Station in its first 6.5 years operation. The AMS electron flux exhibits a significant excess starting from $42.1^{+5.4}_{-5.2}$ GeV compared to the lower energy power law trend. At 5σ significance level, the electron flux does not have an exponential cutoff below 1.9 TeV. In the entire energy range, the electron flux can be described by the sum of two power law components. The distinctive properties in the electron flux provide new understanding of the origins of cosmic ray electrons.

*36th International Cosmic Ray Conference -ICRC2019-
July 24th - August 1st, 2019
Madison, WI, U.S.A.*

*Speaker.

[†]for collaboration list see PoS(ICRC2019)1177

1. Introduction

The precision measurement of the electron flux in the primary cosmic rays from 0.5 GeV to 1.4 TeV with the Alpha Magnetic Spectrometer (AMS) on the International Space Station (ISS) is presented. The measurements are based on 28.1 million electron events collected by AMS from May 19, 2011 to November 12, 2017. The results on the behavior of electron flux at high energies are crucial for understanding the origins of high energy cosmic-ray electrons and positrons.

2. AMS detector and analysis

The description of the AMS detector is presented in Ref. [1] and references therein. The detector performance on orbit is continuously monitored and the overall AMS instrument response stability is $(0.0 \pm 0.4)\%$. For the details of AMS detectors and advances in the analysis methods please refer to upcoming AMS review article.

AMS has collected 1.07×10^{11} cosmic rays in the first 6.5 years of operation. The collection time for galactic cosmic rays increases with rigidity reaching 1.51×10^8 s above 30 GeV. Template fit methods are used to determine the number of electrons in each energy bin. In total, 28.1 million electrons are collected from 0.5 GeV and 1.4 TeV. For the analysis details and particularly the systematic errors please refer to AMS recent publications in PRL [2, 3].

3. Results

The AMS results on the electron spectrum (i.e. the flux scaled with \tilde{E}^3 , $\tilde{E}^3 \Phi_{e^-}$) is presented in Fig. 1 in comparison with the most recent AMS positron spectrum [2]. The spectrally weighted mean energy \tilde{E} is calculated following Ref. [4] for a flux $\propto E^{-3}$. As seen, the electron and positron spectra have distinctly different magnitudes and energy dependencies.

The AMS results on the electron spectrum together with earlier measurements [5, 6, 7, 8, 9, 10, 11] are shown in Fig. 2. The AMS results significantly improve the precision and extend the measurements to the uncharted high energy region.

To examine the energy dependence of the electron flux in a model independent way, the flux spectral index γ is calculated from

$$\gamma = d[\log(\Phi)]/d[\log(E)], \quad (3.1)$$

over non-overlapping energy intervals which are chosen to have sufficient sensitivity to the spectral index. The results are presented in Fig. 3 together with the positron results [2]. As seen, both the electron and positron indices decrease (soften) rapidly with energy below ~ 10 GeV, and then they both start increasing (harden) at > 20 GeV. In particular, the electron spectral index increases from $\gamma = -3.295 \pm 0.026$ in the energy range [17.98 – 27.25] GeV to an average $\gamma = -3.180 \pm 0.008$ in the range [55.58 – 1400] GeV, where it is nearly energy independent. The behavior of the electron and positron spectral indices is distinctly different.

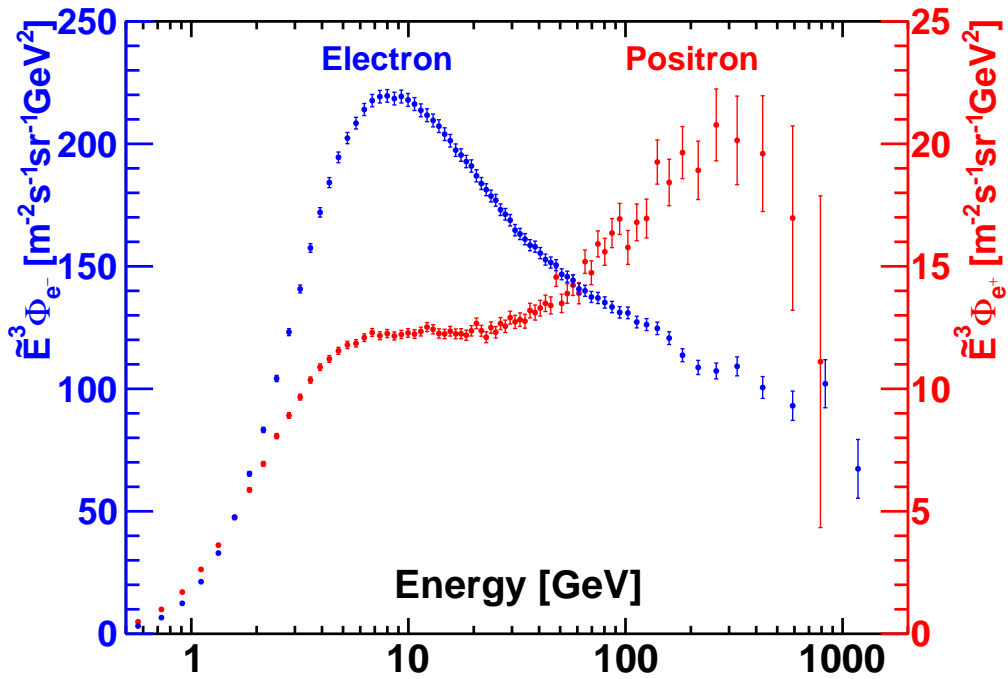


Figure 1: The electron (blue, left axis) and positron (red, right axis) spectra ($\tilde{E}^3 \cdot \Phi_{e^\pm}$). For display purposes the positron data point at ~ 830 GeV is slightly shifted horizontally to avoid overlap with the electron point. As seen, the electron spectrum has distinctly different magnitude and energy dependence compared to that of positrons

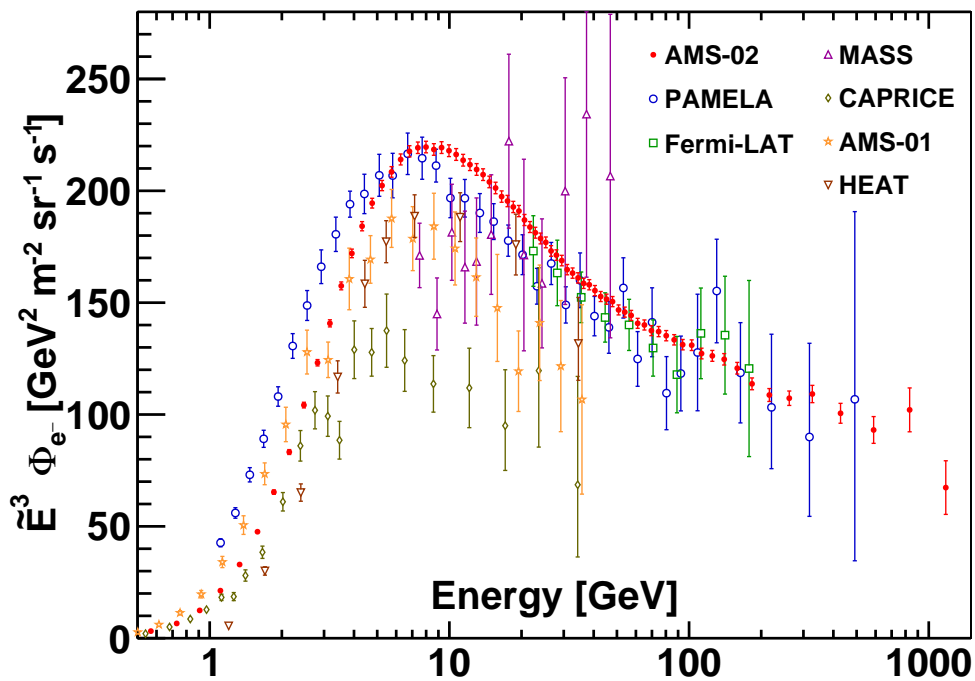


Figure 2: The AMS electron spectrum ($\tilde{E}^3 \cdot \Phi_{e^-}$) together with earlier experiments.

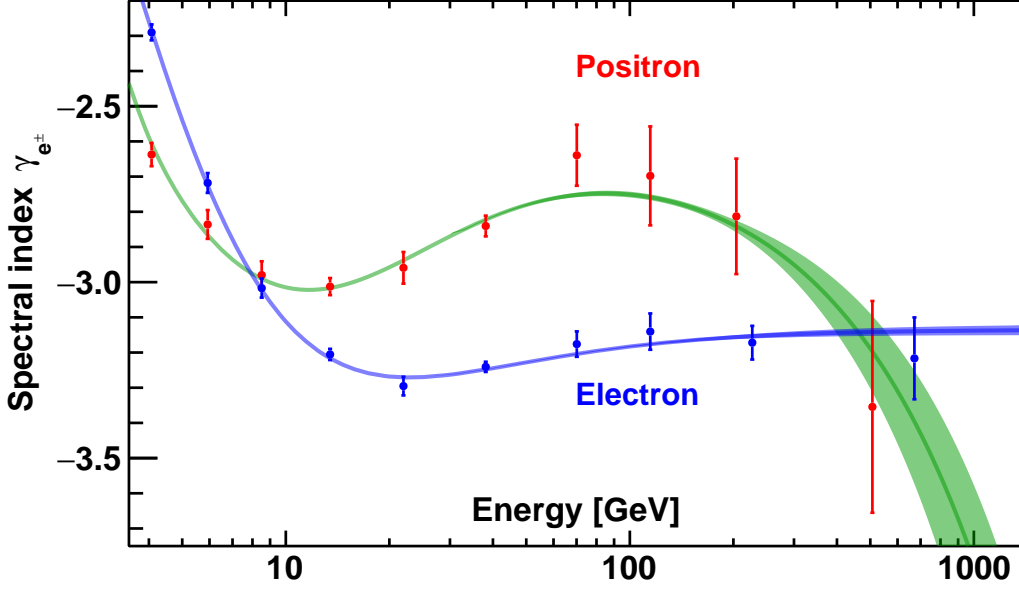


Figure 3: The spectral indices of the electron flux (blue) and positron flux (red) in non-overlapping intervals. They show distinctly different behavior. The blue band represents the 68% C.L. interval of the fit of Eq. (3.5) to the electron flux (see text). The green band represents the 68% C.L. interval of a fit to the positron flux [Eq. (4) in Ref. [2]].

To determine the transition energy E_0 where the change of the electron spectral index occurs, we use a double power law approximation

$$\Phi_{e^-}(E) = \begin{cases} C(E/20.04 \text{ GeV})^\gamma, & E \leq E_0; \\ C(E/20.04 \text{ GeV})^\gamma (E/E_0)^{\Delta\gamma}, & E > E_0. \end{cases} \quad (3.2)$$

A fit to data is performed in the energy range [20.04 – 1400] GeV. The energy range boundary of 20.04 GeV is chosen to be above the observed range of time dependence based on the analysis of Ref. [2]. The results are presented in Fig. 4. The fit yields $E_0 = 42.1^{+5.4}_{-5.2}$ GeV and $\Delta\gamma = 0.094 \pm 0.014$ with $\chi^2/\text{d.o.f.} = 17.9/36$. The energy E_0 corresponds to the beginning of spectral hardening compared to the lower energy trends. The spectral index change by $\Delta\gamma$ is clearly visible in Fig. 4. Note that the choice of the value 20.04 GeV does not affect the fitted values of E_0 , γ , and $\Delta\gamma$.

To investigate the existence of a finite energy cutoff as seen in the positron flux [2], the electron flux is fitted starting from the lower boundary of the E_0 bin [41.61 – 44.00] GeV with

$$\Phi_{e^-}(E) = C_s (E/41.61 \text{ GeV})^{\gamma_s} \exp(-E/E_s). \quad (3.3)$$

A fit to data in the energy range [41.61 – 1400] GeV yields the inverse cutoff energy $1/E_s = 0.00^{+0.08}_{-0.00} \text{ TeV}^{-1}$ with $\chi^2/\text{d.o.f.} = 15.2/23$. A study of the cutoff significance shows that $E_s < 1.9 \text{ TeV}$ is excluded at the 5σ level. These results are presented in Fig. 5.

New sources of high energy positrons, such as dark matter, may also produce an equal amount of high energy electrons. To test the consistency of this assumption with the data in the energy range [41.61 – 1400] GeV, the electron flux is parametrized as a sum of a power law component

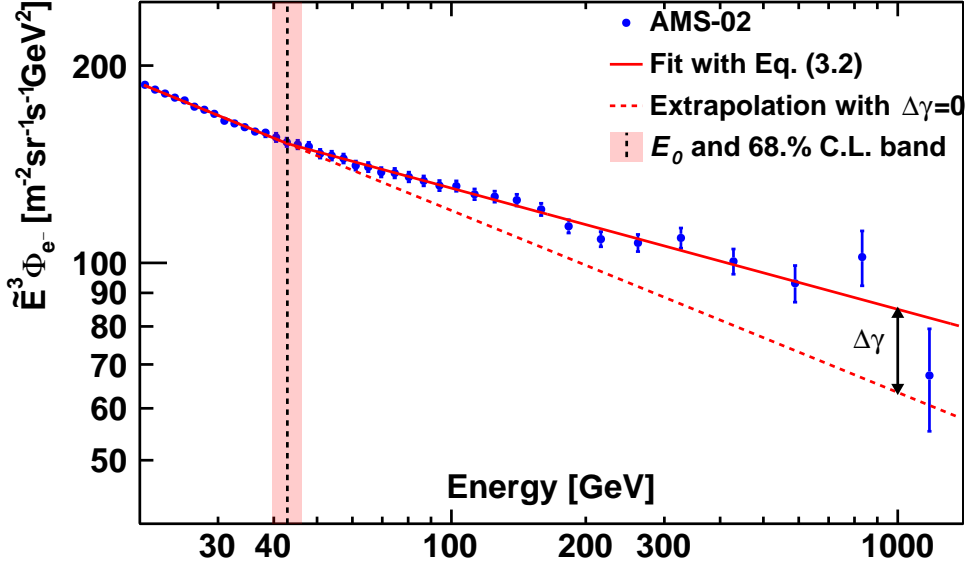


Figure 4: A double power law fit of Eq. (3.2) to the electron flux in the energy range [20.04 – 1400] GeV. The blue data points are the measured electron flux values scaled by \tilde{E}^3 . The fitted function is represented by the solid red line. The vertical dashed line and the red band correspond to the value and the error of the energy E_0 where the change of the spectral index occurs and $\Delta\gamma = 0.094 \pm 0.014$ is the magnitude of the spectral index change, see Eq. (3.2). The dashed red line is the extrapolation of the power law below E_0 into the higher energy region (or $\Delta\gamma = 0$ in Eq. (3.2)).

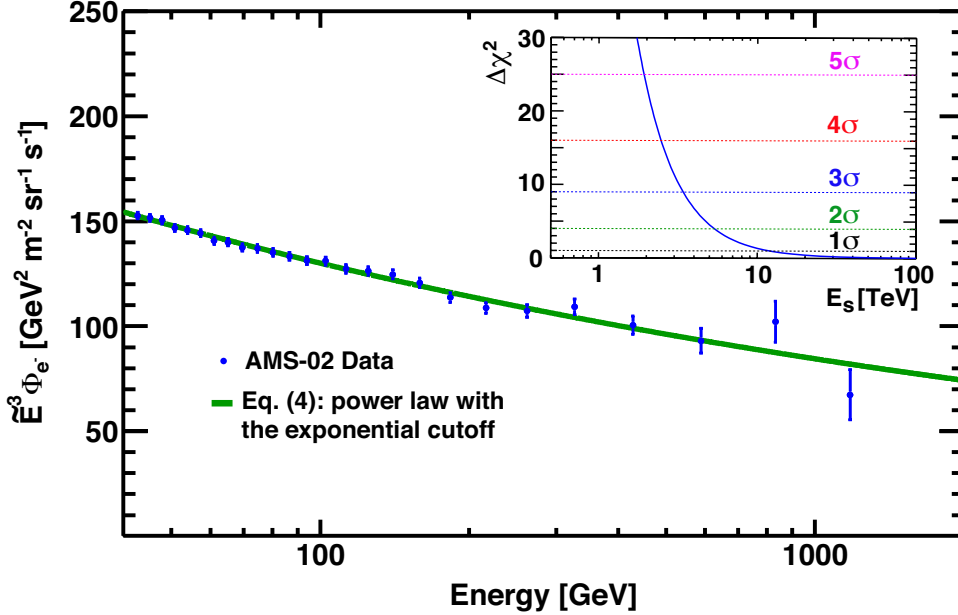


Figure 5: The fit of Eq. 3.3 to the electron flux data in the energy range [41.61 – 1400] GeV. The insert shows the study of the significance of the $1/E_s$ measurement by varying all three fit parameters in Eq. 3.3 to find the minimal $\Delta\chi^2$ corresponding to E_s values from 1 to 100 TeV. The blue curve shows the dependence of $\Delta\chi^2$ on E_s and the horizontal dashed lines show different significance levels from 1 to 5σ . As seen, E_s values below 1.9 TeV are excluded at the 5σ level.

and the identical source term as for positrons [2]:

$$\Phi_{e^-}(E) = C_{e^-} (E/E_1)^{\gamma_{e^-}} + f_{e^-} C_s^{e^+} (E/E_2)^{\gamma_s^{e^+}} \exp(-E/E_s^{e^+}). \quad (3.4)$$

The values of the source term parameters $C_s^{e^+}$, $\gamma_s^{e^+}$, E_2 , and $E_s^{e^+}$ are taken from Ref. [2]. The fit yields $\chi^2/\text{d.o.f.} = 15.5/24$ if f_{e^-} is fixed to 1, and $\chi^2/\text{d.o.f.} = 15.2/24$ if f_{e^-} is fixed to 0 (i.e. no contribution from positron source term). The analysis shows that AMS electron data are consistent both with the charge symmetric positron source term [2] ($f_{e^-} = 1$ in Eq. (3.4)) and also with the absence of such a term ($f_{e^-} = 0$).

Most surprisingly, we found that in the entire energy range [0.5 – 1400] GeV the electron flux is well described by the sum of two power law components:

$$\Phi_{e^-}(E) = \frac{E^2}{\hat{E}^2} [1 + (\hat{E}/E_t)^{\Delta\gamma}]^{-1} [C_a (\hat{E}/E_a)^{\gamma_a} + C_b (\hat{E}/E_b)^{\gamma_b}]. \quad (3.5)$$

The low energy transition term, $[1 + (\hat{E}/E_t)^{\Delta\gamma}]^{-1}$, is introduced to account for the complex spectral behavior of the electron flux at energies below ~ 10 GeV [12, 13]. The two components, a and b , correspond to two power law functions with corresponding normalization factors C_a and C_b , and spectral indices γ_a and γ_b . To account for solar modulation effects, the force-field approximation [14] is used, with the energy of particles in the interstellar space $\hat{E} = E + \phi_{e^-}$ and the effective modulation potential ϕ_{e^-} . The result of the fit is presented in Fig. 6. The energy dependence of the electron spectral index corresponding to the results of the fit of Eq. (3.5) is shown in Fig. 3 as a blue 68% C.L. band.

In the energy range [0.5 – 1400] GeV the sum of two power law functions with the transition term provides an excellent description of the data. These functions are very different in shape and in magnitude from those describing the positron flux [2]. The power law a contribution exceeds the expected secondary electron or positron production by a factor of ~ 20 (see Ref. [15]). The power law b contribution, which dominates the electron flux at high energies > 40 GeV, significantly exceeds the magnitude of the positron source term [2].

The observations discussed above are clear evidences that most cosmic-ray electrons originate from different sources than cosmic-ray positrons.

4. Conclusion

We have presented the high statistics precision measurements of the electron flux from 0.5 GeV to 1.4 TeV, with detailed study of systematic uncertainties based on a data sample of 28.1 million electrons. In the entire energy range the electron and positron spectra have distinctly different magnitudes and energy dependences. The electron flux exhibits a significant excess starting from $42.1_{-5.2}^{+5.4}$ GeV compared to the lower energy trends, but the nature of this excess is different from the positron flux excess above 25.2 ± 1.8 GeV. Contrary to the positron flux, which has an exponential energy cutoff of 810_{-180}^{+310} GeV, at the 5σ level the electron flux does not have an energy cutoff below 1.9 TeV. In the entire energy range from 0.5 GeV to 1.4 TeV the electron flux is well described by the sum of two power law components. The different behavior of the cosmic-ray electrons and positrons measured by AMS is clear evidence that most high energy electrons originate from different sources than high energy positrons.

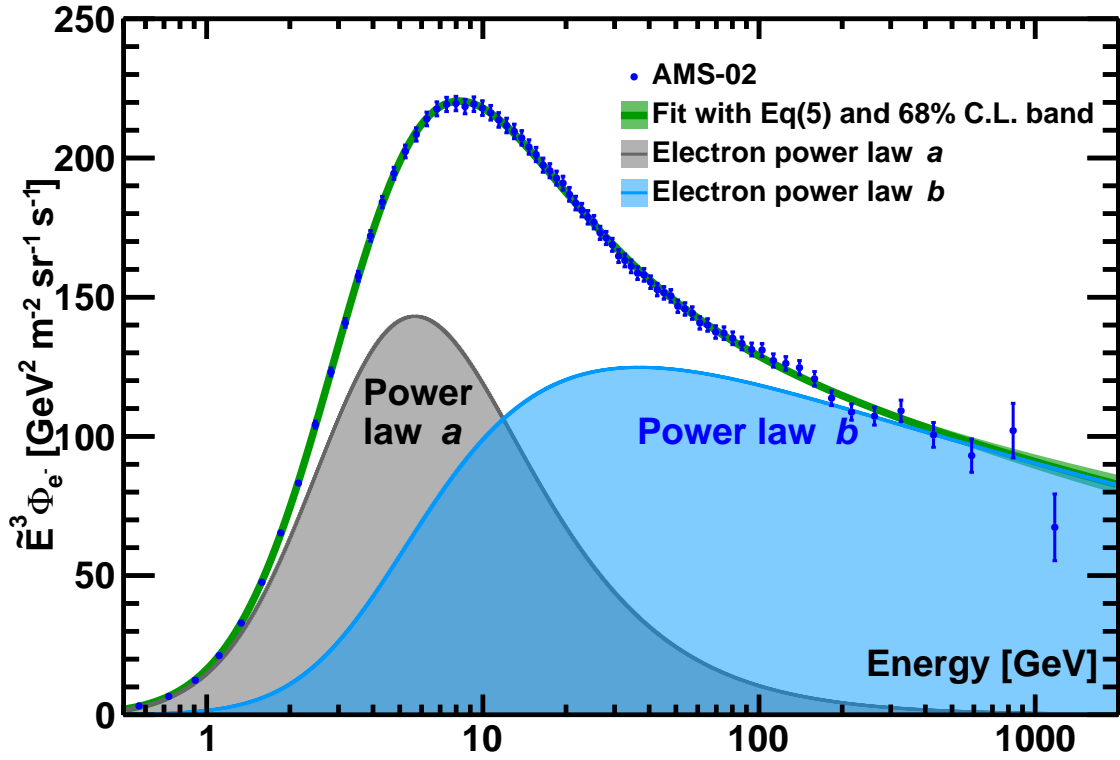


Figure 6: The two power law fit of Eq. (3.5) to the electron flux data in the energy range [0.5 – 1400] GeV with the 68% C.L. (green band). The two power law components a and b of Eq. (3.5) are represented by the gray and blue areas, respectively.

5. Acknowledgments

This work has been supported by acknowledged person and institutions in Ref. [2].

References

- [1] M. Aguilar *et al.*, *Phys. Rev. Lett.* **110**, 141102 (2013);
- [2] M. Aguilar *et al.*, *Phys. Rev. Lett.* **122**, 041102 (2019);
- [3] M. Aguilar *et al.*, *Phys. Rev. Lett.* **122**, 101101 (2019);
- [4] G.D. Lafferty and T.R. Wyatt, *NIM A* **355**, 541 (1995). We have used Eq. (6) with $\tilde{E} \equiv x_{lw}$.
- [5] J. Alcaraz *et al.*, *Phys. Lett. B* **484**, 10 (2000).
- [6] O. Adriani *et al.*, *Phys. Rev. Lett.* **106**, 201101 (2011).
- [7] M. Ackermann *et al.*, *Phys. Rev. Lett.* **108**, 011103 (2012).
- [8] C. Grimani *et al.*, *Astron. Astrophys.* **392**, 287 (2002).
- [9] M. Boezio *et al.*, *Adv. Space Res.* **27**, 669 (2001).
- [10] M. Aguilar *et al.*, *Phys. Lett. B* **646**, 145 (2007).

- [11] S.W. Barwick *et al.*, *Astrophys. J.* **498**, 779 (1998); M.A. DuVernois *et al.*, *Astrophys. J.* **559**, 296 (2001); J.J. Beatty *et al.*, *Phys. Rev. Lett.* **93**, 241102 (2004).
- [12] M. Aguilar *et al.*, *Phys. Rev. Lett.* **121**, 051102 (2018).
- [13] Ł. Stawarz, V. Petrosian, and R. D. Blandford, *Astrophys. J.* **710**, 236 (2010).
- [14] R. A. Caballero-Lopez and H. Moraal, *J. Geophys. Res.* **109**, A01101 (2004); L. Gleeson and W. Axford, *Astrophys. J.* **154**, 1011 (1968).
- [15] I. V. Moskalenko and A. W. Strong, *Astrophys. J.* **493**, 694 (1998); A. E. Vladimirov, S. W. Digel, G. Jóhannesson, P. F. Michelson, I. V. Moskalenko, P. L. Nolan, E. Orlando, T. A. Porter, and A. W. Strong, *Comput. Phys. Commun.* **182**, 1156 (2011).